




# Neutrophil Extracellular Traps Induce Alveolar Macrophage Pyroptosis by Regulating NLRP3 Deubiquitination, Aggravating the Development of Septic Lung Injury

Yamei Cui\*, Ying Yang\*, Wenqiang Tao , Wei Peng, Deqiang Luo , Ning Zhao , Shuangyan Li, Kejian Qian, Fen Liu

Department of Critical Care Medicine, The First Affiliated Hospital of Nanchang University, Nanchang, People's Republic of China

\*These authors contributed equally to this work

Correspondence: Fen Liu, Department of Critical Care Medicine, The First Affiliated Hospital of Nanchang University, No. 17 Yongwaizheng Street, Dong Lake District, Nanchang, 330000, People's Republic of China, Tel +86 0791 88692533, Email liufen9934@163.com

**Background:** Uncontrolled inflammation is a typical feature of sepsis-related lung injury. The key event in the progression of lung injury is Caspase-1-dependent alveolar macrophage (AM) pyroptosis. Similarly, neutrophils are stimulated to release neutrophil extracellular traps (NETs) to participate in the innate immune response. This study aims to illustrate the specific mechanisms by which NETs activate AM at the post-translational level and maintain lung inflammation.

**Methods:** We established a septic lung injury model by caecal ligation and puncture. We found elevated NETs and interleukin-1 $\beta$  (IL-1 $\beta$ ) levels in the lung tissues of septic mice. Western blot and immunofluorescence analyses was utilized to determine whether NETs promote AM pyroptosis and whether degrading NETs or targeting the NLRP3 inflammasome had protective effects on AM pyroptosis and lung injury. Flow cytometric and co-immunoprecipitation analyses verified intracellular reactive oxygen species (ROS) levels and the binding of NLRP3 and ubiquitin (UB) molecules, respectively.

**Results:** Increased NETs production and IL-1 $\beta$  release in septic mice were correlated with the degree of lung injury. NETs upregulated the level of NLRP3, followed by NLRP3 inflammasome assembly and caspase-1 activation, leading to AM pyroptosis executed by the activated fragment of full-length gasdermin D (FH-GSDMD). However, the opposite effect was observed in the context of NETs degradation. Furthermore, NETs markedly elicited an increase in ROS, which facilitated the activation of NLRP3 deubiquitination and the subsequent pyroptosis pathway in AM. Removal of ROS could promote the binding of NLRP3 and ubiquitin, inhibit NLRP3 binding to apoptosis-associated spotted proteins (ASC) and further alleviate the inflammatory changes in the lungs.

**Conclusion:** In summary, these findings indicate that NETs prime ROS generation, which promotes NLRP3 inflammasome activation at the post-translational level to mediate AM pyroptosis and sustain lung injury in septic mice.

**Keywords:** sepsis, neutrophil extracellular traps, macrophage pyroptosis, NLRP3 inflammasomes, ubiquitination, oxidative stress

## Introduction

Sepsis is a life-threatening clinical syndrome. The main characteristic is the uncontrollable organismal response to invading pathogens, leading to multiple organ dysfunction.<sup>1</sup> The lungs bear the brunt of inflammation; almost half of septic patients will develop acute lung injury (ALI) and acute respiratory distress syndrome (ARDS), and the mortality rate is approximately 60%.<sup>2-4</sup> Moreover, infiltrating neutrophils cluster in lung tissue during sepsis-induced ALI.<sup>5</sup> In addition to performing degranulation and phagocytosis, activated neutrophils release neutrophil extracellular traps (NETs), a DNA network structure composed of 15 to 17 nm chromatin fibres on which histones, myeloperoxidase (MPO), and other antibacterial proteins are attached; NETs release is regarded as a novel extracellular effector

mechanism of neutrophils to combat pathogenic microorganisms.<sup>6,7</sup> Phorbol 12-myristate 13-acetate (PMA) is commonly used to induce NETs production *in vitro*.<sup>8</sup> In addition, lipopolysaccharide (LPS), platelets, bacteria, viruses, fungi, the cytokine IL-8, and crystals have been reported to promote NETs release.<sup>7,9,10</sup> However, recent studies have reported that NETs have cytotoxic and proinflammatory effects that drive the development of inflammatory diseases, such as diabetes, sepsis-related lung injury, atherosclerosis, and systemic lupus erythematosus.<sup>11–14</sup> For example, the severity and mortality of ARDS were associated with increased NETs levels, although deoxyribonuclease I (DNase 1) could mitigate the severity and mortality of ARDS but was associated with the risk of an increased bacterial load.<sup>15,16</sup> Therefore, given the dual roles of NETs in sepsis, clarifying how NETs induce the exacerbation of septic lung injury remains to be explored.

Pyroptosis, which separately depends on caspase-1 participating in the canonical pyroptosis pathways and caspase-11 (or caspase-4/5) mediating the non-canonical pyroptosis pathway, is a programmed cell death process amplified by an inflammatory cascade; this process is documented to occur mainly in dendritic cells and macrophages.<sup>17</sup> The chief feature of pyroptotic cells is the swelling and rupture of the cell membrane, which leads to the release of interleukin (IL)-1 $\beta$  and IL-18. This process is executed by N-terminal gasdermin D (N-GSDMD) generated by the cleavage of GSDMD and subsequent oligomerization to form 1- to 2-nm pores on the surface of the cell membrane.<sup>18</sup> Moreover, compromised cell membranes allow annexin V to bind with phosphatidyl serine (PS) in pyroptotic cells.<sup>17</sup> Furthermore, almost all inflammatory caspases are activated within an inflammasome complex.<sup>19</sup> The NLRP3 inflammasome has received extensive attention due to its involvement in the progression of many diseases. NLRP3 interacts with the apoptosis-associated spotted protein (ASC) molecule to form ASC foci, further recruiting and activating caspase-1 to form a complete inflammasome complex.<sup>20</sup> However, both treatment with the NLRP3 inhibitor MCC950 and knockout of NLRP3 were found to significantly reduce the lung inflammation induced by LPS *in vivo*.<sup>21,22</sup> Therefore, the activation of NLRP3 is a prerequisite for NLRP3 inflammasome assembly and pyroptosis.

NLRP3, a subset of the nucleotide binding and oligomerization domain (NOD)-like receptors (NLRs), can widely sense a diverse range of irritants inside and outside the human body, including pathogenic microorganisms, bacterial toxins, asbestos, uric acid, cholesterol, and ATP.<sup>11,23</sup> Moreover, multiple studies have shown that NETs act as danger-associated molecular patterns (DAMPs) to activate the NLRP3 inflammasome,<sup>24</sup> but the specific mechanism has not been elucidated. In addition, increasing evidence suggests that the ubiquitin (UB) proteasome system influences the assembly of NLRP3 inflammasome complexes.<sup>25</sup> Moreover, deubiquitination of NLRP3 plays a vital role in NLRP3 inflammasome activation. When deubiquitinases are knocked out or antagonized with inhibitors, there are significant reductions in caspase-1 activity and IL-1 $\beta$  secretion in macrophages.<sup>26–28</sup> In addition, recent studies have reported that reactive oxygen species (ROS) production may be an essential bridge for activating the NLRP3 inflammasome.<sup>29</sup> The accumulation of ROS can affect the binding of NLRP3 to ubiquitin.<sup>30</sup> Surprisingly, when ROS were eliminated with N-acetylcysteine (NAC), NLRP3 ubiquitination resumed, and the expression level of inflammasome-associated proteins was markedly decreased.<sup>31</sup>

Studies have shown that NETs are engulfed and degraded by macrophages, partly through a process mediated by the advanced glycation end products (RAGE) receptor.<sup>32</sup> Based on the above reports, we hypothesized that NETs stimulate macrophages to generate large amounts of ROS, which act as “activation signals” to regulate the activation of NLRP3 at the post-translational modification level, thereby promoting the assembly of NLRP3 inflammasomes and the cleavage of downstream GSDMD to induce alveolar macrophage (AM) pyroptosis; this process provides a new idea for the pathogenesis of sepsis-induced lung injury.

## Materials and Methods

### Animals

The animal experimental procedures and protocols were approved by the ethics committee of the medical innovation centre of the First Affiliated Hospital of Nanchang University (Approval No: CDYFY-IACUC-202208QR009) and performed adherence to the principles and procedures of the National Institutes of Health (NIH) Guide for the Care and Use of Laboratory Animals and the Guidelines for Chinese Regulation for the Use and Care of Laboratory Animals. CRISPR-mediated NLRP3 knockout and GSDMD knockout mice were produced by Beijing View Solid Biotechnology,

China (certificate of conformity: SCXK2016-0009). C57BL/6 mice (8 weeks old; 18–22 g), Sprague-Dawley (SD) Rats (8 weeks old; 100–110 g) were purchased from Hunan SJA Laboratory Animal Corporation, China (certificate of conformity: SCXK2016-0002). According to the regulations of the institution, the mice were fed pathogen-free food and water under standard conditions (12 light/dark rhythm, 25–27 °C, humidity of ~40%).

## Cell Culture

Rat alveolar macrophages (NR8383 cells) purchased from the Chinese Academy of Sciences Cell Bank (Shanghai, China) were cultured in Ham's F-12K complete medium (Boster, China) containing 15% foetal bovine serum (FBS, Gibco, Grand Island, USA) at 37 °C in 95% air and 5% CO<sub>2</sub>. The cells were added to a 6-well plate ( $5 \times 10^5$  cells/mL) overnight. First, cells were induced by 500 ng/mL lipopolysaccharide (LPS, Escherichia coli 055: B5, Sigma–Aldrich) for 2 h and then cocultured with NETs up to 12 h together with or without DNase 1 (100 U/mL, Roche, USA), NLRP3 inhibitor MCC950 (100 nM, MedChemExpress, USA), ROS inhibitor NAC (10 mM, MedChemExpress, USA), Deubiquitinating enzymes inhibitor G5 (1 μM, MedChemExpress, USA), and GSDMD inhibitor Disulfiram (10 μM, MedChemExpress, USA).

## The Establishment of the CLP Model

As previously described, the caecal ligation and puncture (CLP) method was carried out in mice.<sup>33</sup> First, after anaesthetization and disinfection with betadine solution, we performed laparotomy in the abdomen to expose the caecum and the adjoining intestine of mice. Then, a 6.0 thread suture was used to tightly ligate the intestinal canal under the ileocaecal section, puncture the canal wall with a 19-gauge needle, and gently squeeze a small number of intestinal contents into the abdominal cavity to establish a mouse sepsis model. Finally, the mice were subcutaneously injected 1mL saline for post-operative resuscitation. Mice in the sham group underwent laparotomy techniques without ligation and puncture. The ROS scavenger NAC (20 mg/kg) or vehicle was intraperitoneally injected into C57BL/6 mice 1 hour before CLP surgery.

## DNase I Treatment

C57BL/6 mice were randomized and intraperitoneally administered DNase 1 (100 U/mouse, Roche, USA) or vehicle control at 24h before CLP to abrogate NETs formation in septic lung tissues.

## PMNs Isolation in vitro

Neutrophils were isolated from SD rats by a peripheral blood neutrophil isolation kit (Solarbio, Beijing, China) following the manufacturer's specifications. Fresh whole blood was collected and covered in the surface of the separation liquid, and cell pellets were obtained after centrifugation at room temperature. Then, neutrophils were resuspended in 1640 medium (Solarbio, China) incorporating 5% FBS (FBS, Gibco, Grand Island, USA). Neutrophils obtained from peripheral blood (definitely > 95%) were identified by Giemsa staining (Solarbio, China), and cell viability (> 95%) was validated by trypan blue staining (Solarbio, China).

## The Induction and Purification of NETs

100nM phorbol-12-myristate-13-acetate (PMA, Sigma, USA) was used to stimulate neutrophils ( $1 \times 10^7$ /well) grown in 6-well plates for NETs generation at 37 °C in 5% CO<sub>2</sub> for 4 h with or without DNase I. Then, NETs were purified as previously described.<sup>34</sup> After incubation, washed the wells with cold PBS and collected all the supernatant solution. Then, the remaining neutrophils were removed by low-speed centrifugation at 4 °C, and the solution was further centrifuged to purity NETs for subsequent experimental operation.

## Immunofluorescence Staining

Fresh lung tissue was fixed with 4% paraformaldehyde (PFA), dehydrated in a sucrose solution gradient, wrapped with Tissue-Tek OCT, and sectioned into 5-μm slices. In addition, PMNs or NR8383 cells were seeded over a 14-mm coverslip (Solarbio, Beijing) in 24-well plates overnight. Immediately afterwards, cell and tissue slices were fixed in 4% PFA, permeabilized, blocked with 5% goat serum to minimize nonspecific staining, and incubated with the following

primary antibodies overnight at 4 °C. Rabbit polyclonal anti-citrullinated histone H3 (cit-H3, 1:250, Abcam, UK), rat polyclonal anti-LY6G (1:150, Abcam, UK), mouse monoclonal anti-ASC (1:100, Santa Cruz Biotechnology, USA), mouse polyclonal anti-CD68 (1:200, Immunoway Biotechnology, UK), rabbit polyclonal anti-NLRP3 (1:200, Boster, China) and mouse monoclonal anti-ubiquitin (1:100, Santa Cruz Biotechnology, USA) antibodies. Following incubation with secondary Alexa Fluor 488 (1:200, Elabscience, China) and Alexa Fluor 594 (1:200, Elabscience, China) for 1 h at room temperature. The nucleus was stained with 4',6-diamidino-2-phenylindole (DAPI, Boster, China) for 5 min, protected from light. In addition, NETs-associated DNA was detected with SYTOX green in accordance with the manufacturer's specifications. Samples were visualized by confocal laser scanning microscopy (Olympus) or fluorescence microscopy (Zeiss).

## Western Blotting

Protein was extracted from lysis buffer containing a protease inhibitor, and the level of protein was quantified with a protein quantification kit (TransGen Biotech, Beijing, China). Then, equivalent protein samples were separated by SDS-PAGE gels and transferred onto PVDF membranes (Merck Millipore, Darmstadt, Germany), which were blocked in Protein-free fast blocking solution (Boster, China) and cultivated with primary antibody for 12h at 4 °C. After washing three times with wash buffer, the membrane was incubated with the horseradish peroxidase (HRP)-conjugated secondary antibody for 1 h at 37°C. Protein bands were intuitively visualized by an enhanced chemiluminescence (ECL) imaging system (Bio-Rad Laboratories, CA, USA) and quantified with ImageJ software (Rawak Software Inc., Germany). Principal primary antibodies were as follows: rabbit polyclonal anti-CitH3 (1:1000, Abcam, UK), rabbit polyclonal anti-NLRP3 (1:1000, Abcam, UK), rabbit polyclonal anti-GSDMD (1:1000, Cell single Technology, USA), rabbit polyclonal anti-caspase-1 (1:1000, Abcam, UK), rabbit polyclonal anti-H3 (1:1000 dilution, Immunoway Biotechnology, USA), rabbit polyclonal anti-caspase-1 p20 (1:500, Novus Biologicals LLC, USA), and rabbit polyclonal anti-GAPDH (1:1000, Proteintech, China).

## Coimmunoprecipitation

Cells were lysed in equal proportions of immunoprecipitation (IP) buffer (Beyotime, China) with a complete protease inhibitor cocktail (MedChemExpress, USA) on ice for 30 minutes. After centrifugation, the protein samples were acquired and prepared for immunoprecipitation assays. Protein A/G magnetic beads (MedChemExpress, USA) were initially coupled to anti-NLRP3 antibodies (1:30, Abcam, UK) and rotated for 2 hours at 4 °C. After washing three times, 800 µg of total protein was added and corotated with antibody magnetic bead complex overnight at 4 °C. Additionally, the equivalent cognate IgG antibody were used as IP controls. Ultimately, the immunoprecipitated proteins were dissolved in 30 µL 1 x loading buffer (Solarbio, China) by boiling at 10 min for Western blot assay.

## NLRP3 Ubiquitination Detection

The NLRP3 ubiquitylated state was detected as described.<sup>35</sup> MG132 (10 mM, Abmole Bioscience, USA) was added 6 h before sample collection. Cells were lysed in RIPA buffer containing 10 mM N-ethylmaleimide (MedChemExpress, USA) and protease inhibitor cocktail. Then, the interaction between NLRP3 and ubiquitin was detected by immunoprecipitation and immunoblot assays. The primary antibodies were rabbit anti-NLRP3 (1:30, Abcam, USK) and mouse anti-ubiquitin (1:500, Santa Cruz Biotechnology, USA).

## H&E Staining and Histopathological Analysis

The mice were sacrificed after anaesthetization, and fresh lungs were collected, fixed in 4% PFA buffer, embedded, and sliced into 5-µm thick sections. Then, the slices were stained with haematoxylin and eosin for lung injury assessment. HE-stained images were captured by microscopy (ZEISS) and viewed by two pathologists to evaluate the degree of lung injury as previously reported.<sup>9</sup>



## Immunohistochemical Staining

Lung tissue sections were thoroughly deparaffinized, rehydrated, and placed in citrate buffer (pH=6) for antigen retrieval. Then, the sections were incubated in 3% hydrogen peroxide buffer to eliminate endogenous peroxidase. The tissues were blocked at room temperature and subsequent incubation with rat polyclonal anti-LY6G (1:150, Abcam, UK), mouse polyclonal anti-CD68 (1:200, Immunoway Biotechnology, USA), and rabbit polyclonal anti-NLRP3 (1:200, Boster, China) overnight at 4 °C, rinsed three times and incubated with secondary antibody. Images were obtained utilizing an ordinary microscope after counterstaining with 3,3'-diaminobenzidine (DAB) staining (ZSGB-BIO, China). The immunohistochemical (IHC) positive staining area was analyzed by Image-Pro Plus 6.0 software (Media Cybernetics, USA) to assess average optical density (AOD).<sup>36</sup>

## Enzyme-Linked Immunosorbent Assay (ELISA)

ELISA analysis was performed to assess inflammatory cytokines as instructed by the manufacturers. The specific ELISA kits were purchased from Boster (Wuhan, China). The level of interleukin-1b (IL-1 $\beta$ ) in the mouse serum and BALF harvested from each group were detected by commercial mouse IL-1 $\beta$  kits. IL-18, IL-1 $\beta$ , and TNF- $\alpha$  release levels in the supernatants were measured by using specific rat ELISA kits.

## Lactate Dehydrogenase (LDH) Release

The release of LDH into the supernatant was considered a standard cytotoxicity indicator as described previously.<sup>37</sup> After the specific treatments, the culture supernatants were harvested, and LDH levels were detected using the LDH release Assay Kit (Nanjing Jiancheng Bioengineering Institute, China). Subsequently, the absorbance of each sample was measured in a microplate reader (Thermo Fisher Scientific, USA), and its concentration was further calculated.

## Flow Cytometry Detects Programmed Cell Death

The quantification of programmed cell death was accomplished by flow cytometry with a cell death detection kit (4A Biotech Co., Ltd., Beijing, China). The cell suspension was collected and centrifuged at 1000 r for 5 min. After washing with prechilled PBS, the cell agglomerates were resuspended in 500ul binding buffer and adjusted to  $2 \times 10^5$  cells/mL. Two fluorescent dyes were added successively and coincubated with the cell suspension in the dark. The double-stained positive cells for annexin-V and PI were examined in a Mindray Bricyte E6 instrument (Mindray, China).

## Microscope Analysis for Alveolar Macrophage Pyroptosis

Following the manufacturer's instructions, alveolar macrophage pyroptosis was detected by the FAM-FLICA Caspase-1 Detection Kit (Immunochemistry Technologies, Minnesota, USA). The cells were gently collected and cocultured with the caspase-1 fluorescent probe in the dark at 37 °C for 1 h. Washing with 1X apoptosis wash buffer for removing from unbound FLICA in cells. Then, the nucleus was counterstained with Hoechst 33,342 and PI sequentially. The morphology of pyroptotic AM was identified by microscopy and analyzed with ZEN 3.1 software (Carl Zeiss).

## Intracellular ROS Production

A ROS assay kit (Elabscience, China) was used to detect ROS generation in AM. Concisely, cell suspensions collected from the different groups were incubated with 10  $\mu$ M 2',7-dichlorodihydrofluorescein diacetate (DCFH-DA) protected from light at 37 °C for 30 min followed by washing with PBS buffer to remove excess fluorescence probe. Hoechst 33,342 was performed to stain the active cell nucleus. Inverted fluorescence microscopy (Carl Zeiss) and flow cytometry were applied to test the fluorescence intensities in AM.

## Statistical Analysis

All data were analyzed using SPSS version 26.0 (IBM, USA), and statistical charts were generated using GraphPad Prism 8 software. The statistical methods of unpaired Student's *t*-test and one-way analysis of variance (ANOVA) were

used to assess between-group differences. A value of  $P < 0.05$  was defined as statistically significant. Quantitative data are presented as the mean  $\pm$  standard deviation (SD) from three independent measurements.

## Results

### Sepsis Primes NETs Formation and IL-1 $\beta$ Secretion to Aggravate Lung Injury

After establishing a caecal ligation and puncture (CLP) method, lung tissues were separated from mice in each group. Activated neutrophils infiltrate lung tissue and release decondensed chromatin and proteins to fix and kill pathogens.<sup>6</sup> Immunofluorescence assays were performed to assess LY6G and Citrullinated histone H3 (CitH3) double staining, which reflected NETs production in the lung tissues of septic mice (Figure 1A). NETs-associated DNA was detected with the SYTOX green nucleic acid stain (Figure 1B). The results indicated that the release of NETs was considerably increased in the CLP group compared with the sham group. However, DNase 1 treatment remarkably digested the chromatin structure to effectively restrain NETs formation (Figure 1A and B). Moreover, the protein expression of citH3 also supported the above conclusion (Figure 1C). In addition, characteristic pathological alterations in lung tissue, including immune cell infiltration, pulmonary oedema, and alveolar haemorrhage, were observed in the CLP group, and these effects could be inhibited with DNase 1 treatment (Figure 1D and E). The lung wet-to-dry (W/D) ratio was used to reflect the severity of pulmonary oedema (Figure 1F). Furthermore, the levels of bronchoalveolar lavage fluid (BALF) or serum IL-1 $\beta$  measured by enzyme-linked immunosorbent assay (ELISA) were significantly higher in mice in CLP group than in those in the sham group and were discernibly decreased after treatment with DNase I ( $p < 0.01$ ) (Figure 1G and H). Together, neutrophils in septic mice actively primed NETs production, and the level of IL-1 $\beta$  was partially affected by NETs.

### NETs Could Promote an Inflammatory Response in Macrophages

Macrophages are primarily immune cells in the lungs. We observed that most LY-6G-positive neutrophils were recruited into lung tissues 24 h post CLP, as assessed by immunohistochemical (IHC) staining (Figure 2A). Likewise, the number of CD68-positive macrophages was increased significantly in the CLP group compared to the sham group (Figure 2B). Surprisingly, the immunofluorescence assay revealed that macrophages (red) and neutrophils (green) in lung tissues were adjacent in the CLP group (Figure 2C), raising the possibility that macrophages and NETs were jointly involved in sepsis-induced lung injury. We isolated peripheral blood neutrophils from wild-type (WT) rats, and neutrophil morphology and activity were verified by Giemsa staining and trypan blue staining, respectively (Figure 2D and E). Then, we stimulated neutrophils with PMA (100 nM) with or without DNase I (100 U/mL) for up to 4 h to induce NET formation. The production of NETs was identified by extracellular DNA (green) and citH3 (red) double staining observed by fluorescence microscopy, as shown in Figure 2F, while NETs can be degraded by DNase I in vitro. To investigate whether NETs directly regulate cytokine production in macrophages, LPS-primed NR8383 cells were exposed to NETs for 12 h in the presence or absence of DNase I, and then the supernatant was collected for ELISA analysis. Treatment with NETs plus LPS significantly induced the release of IL-1 $\beta$  and IL-18 compared with the LPS or control treatment ( $p < 0.01$ ) (Figure 2G and H), but there was no significant change in TNF- $\alpha$  ( $p > 0.05$ ) (Figure 2I). However, DNase I inhibited the production of these cytokines (Figure 2G and H). In conclusion, these results indicate that NETs could have a promoting effect on the inflammatory response of alveolar macrophages (AM).

### NETs Induce AM Pyroptosis by Activating the NLRP3 Inflammasome

GSDMD is an executor of pyroptosis, and the N-terminal fragment of GSDMD is required for IL-1 $\beta$  secretion.<sup>18</sup> To confirm that NETs could induce AM pyroptosis in vitro. LPS-primed NR8383 cells were exposed to NETs for up to 12 h. Western blot analysis of the expression levels of NLRP3, caspase-1, GSDMD, N-GSDMD, and caspase-1 p20 in the individual groups was performed. We found that LPS + NETs significantly elevated the levels of NLRP3, N-GSDMD, and caspase-1 p20 in cells ( $p < 0.01$ ) (Figure 3A). Similarly, the expression of IL-1 $\beta$  and IL-18 but not that of TNF- $\alpha$  ( $p > 0.05$ ) in the LPS+NETs group was found to be considerably increased by using ELISA ( $p < 0.01$ ) (Figure 3B). In addition, the combination of LPS plus NETs remarkably promoted lactate dehydrogenase (LDH) release in NR8383 cells

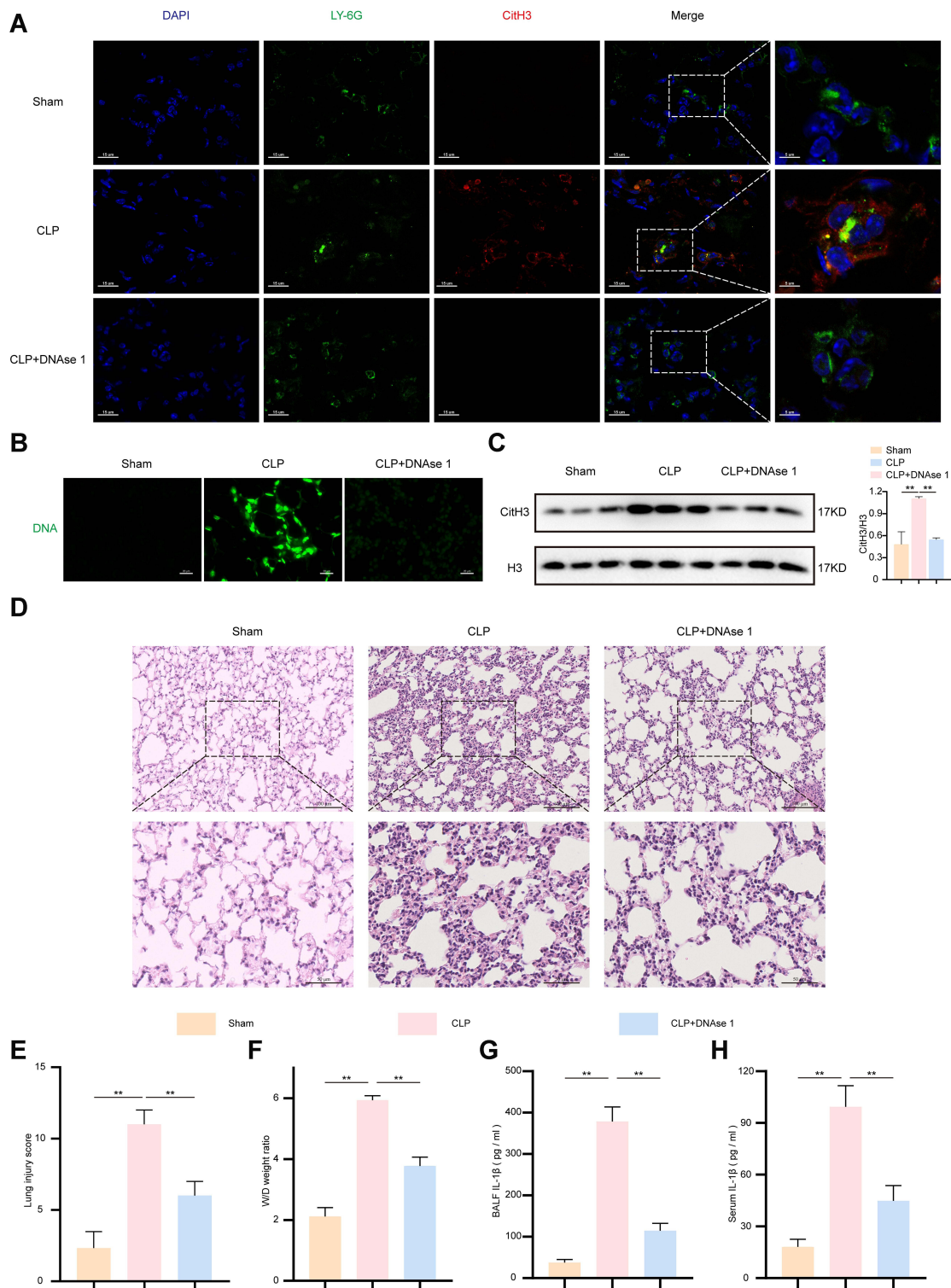


**Figure 1** Elevated IL-1 $\beta$  and NETosis were observed in sepsis-induced lung injuries. After DNase I was administered intraperitoneally for 24 hour, the mice were subjected to CLP for 24 h (n = 6). The sham group was used as a control. Then, the mice were sacrificed, and lung tissues were collected for further analysis. **(A)**. Representative confocal images of Ly6G (green) and CitH3 (red) immunofluorescent staining revealed NETs formation in lung tissues samples. DAPI (blue) was used to stain the cell nuclei. Scale bars, 15  $\mu$ m and 5  $\mu$ m. **(B)**. NETs associated DNA components were stained with SYTOX Green. Scale bar, 20  $\mu$ m. **(C)**. CitH3 protein expression levels were detected by Western blot in tissue lysate. H3 was regarded as a reference protein. **(D and E)**. Representative images of haematoxylin and eosin staining-stained lung tissues and lung injury score from indicated groups. Scale bars, 50  $\mu$ m and 100  $\mu$ m. **(F)**. Pulmonary edema was evaluated by the lung W/D ratio. **(G and H)**. ELISA was used to measure the BALF and serum IL-1 $\beta$  in mice. For all experiments, data are presented as the mean  $\pm$  SD, one-way ANOVA was used for statistical analysis, \*\* $P < 0.01$ . **Abbreviation:** ns, not significant ( $p > 0.05$ ).

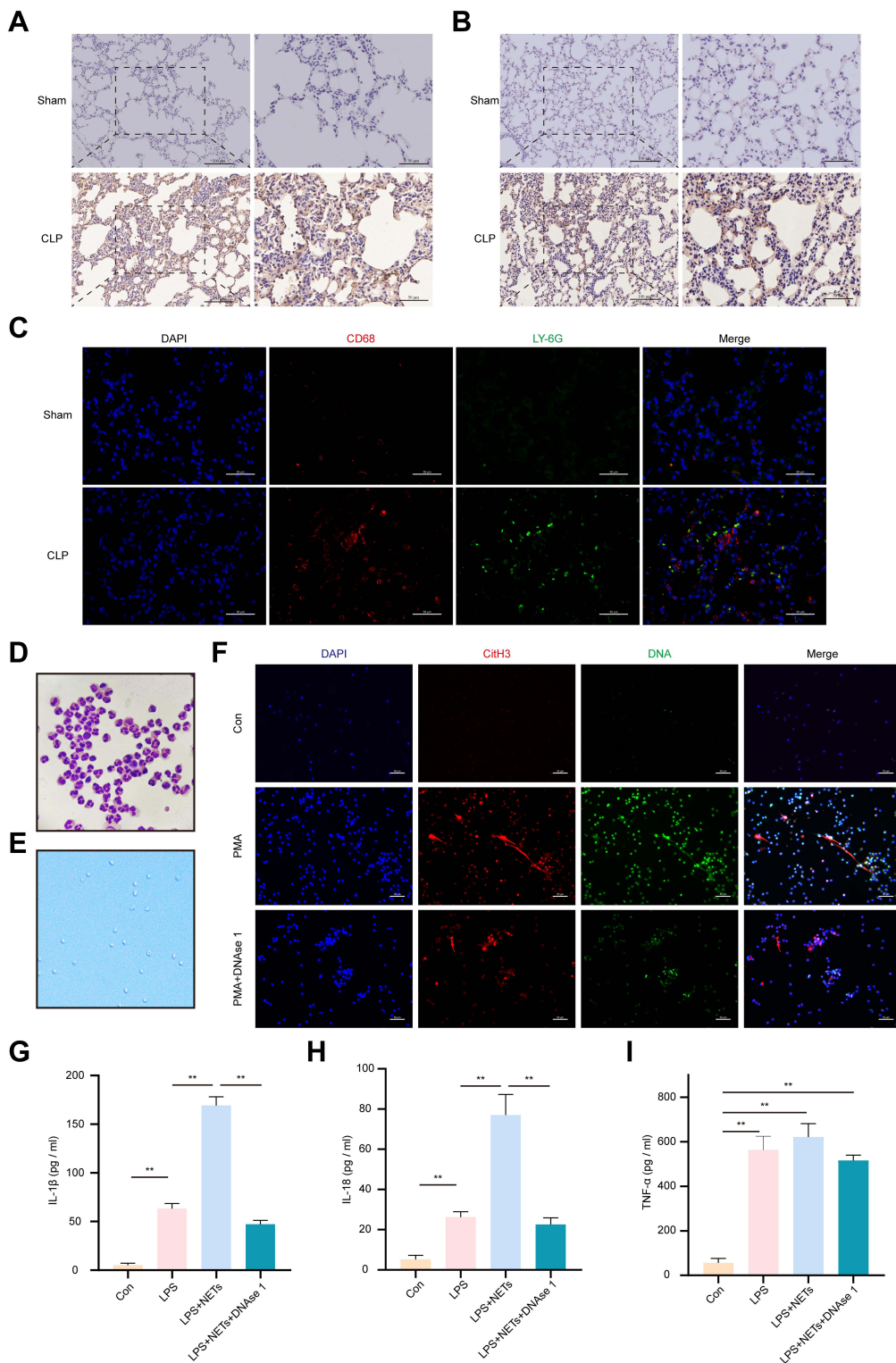


**Figure 2** NETs promote the inflammatory response of macrophages. **(A and B)** Representative immunohistochemistry staining of LY6G-positive neutrophils and CD68-positive macrophages infiltrated the lung tissues in the CLP group. Scale bars, 50  $\mu$ m and 100  $\mu$ m. **(C)** Both neutrophils (Ly6G, green) and macrophages (CD68, red) were detected in the lung sections of the CLP model. Scale bars, 50  $\mu$ m. **(D)** The purity of rat peripheral neutrophils was >95%, as determined by Wright–Giemsa staining (magnification, 1000 $\times$ ). **(E)** Neutrophil viability was detected by trypan blue staining (magnification, 100 $\times$ ). Rat PMNs were stimulated with 100 nmol/L PMA for 4 h to induce NETs formation with or without DNase I. **(F)** The release of NETs was confirmed with SYTOX green and CitH3 staining (red) in each group. Images were obtained by fluorescence microscopy. Scale bar, 50  $\mu$ m. LPS-pretreated NR8383 cells were stimulated with PBS, NETs, or NETs coincubated with DNase I. **(G–I)** ELISA was used to assess IL-1 $\beta$ , IL-18, and TNF- $\alpha$  in the supernatant. For all experiments, data are presented as the mean  $\pm$  SD, one-way ANOVA was used for statistical analysis, \*\* $P < 0.01$ . **Abbreviation:** ns, not significant ( $p > 0.05$ ).



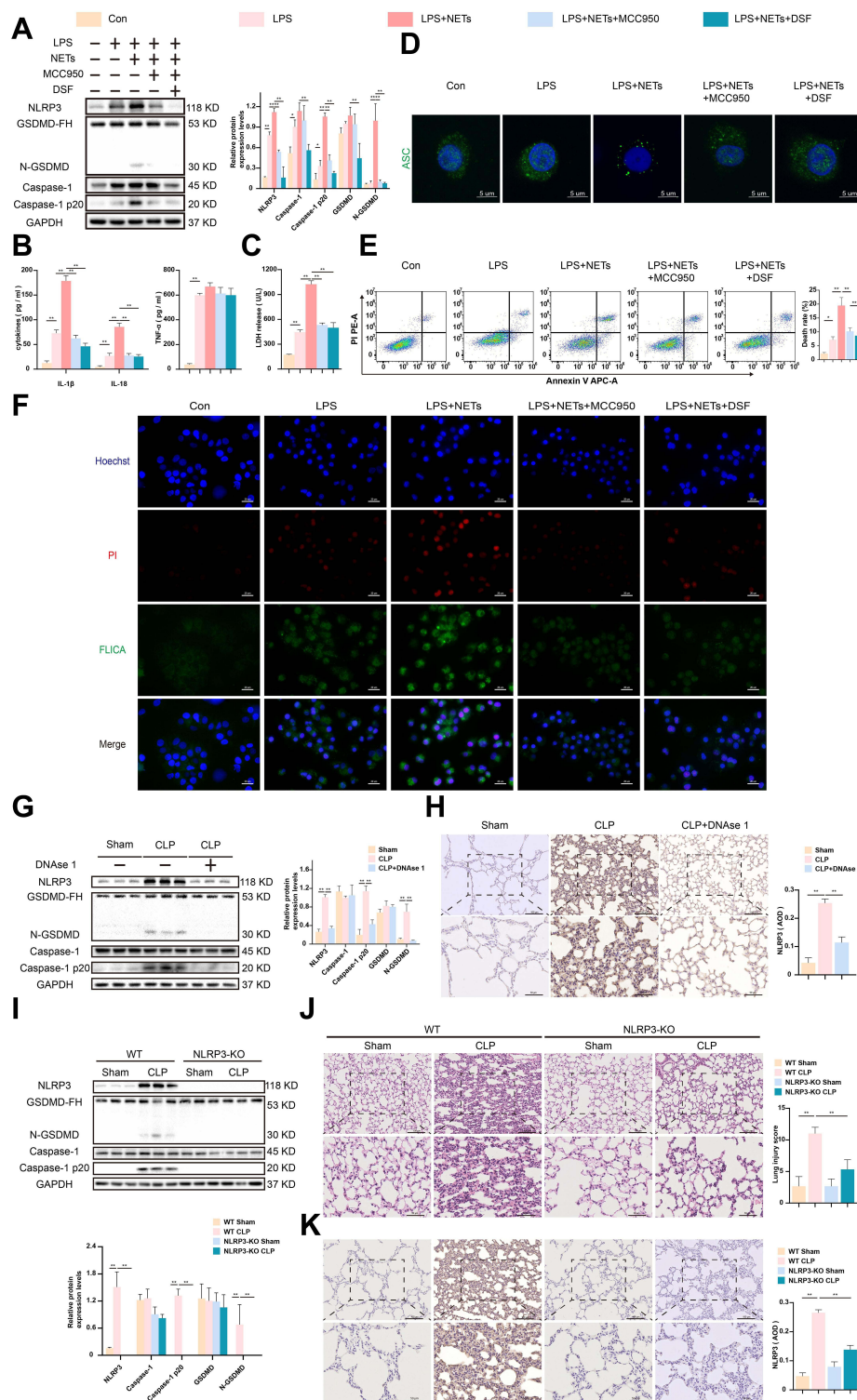


**Figure 3** NETs activate the NLRP3 inflammasome to induce alveolar macrophage pyroptosis. LPS-primed NR8383 cells were induced by NETs for 12 h, MCC950 or DSF was added 30 min prior to NETs. **(A)** Western blot showing the protein levels of NLRP3, caspase-1, caspase 1 p20, GSDMD (GSDMD-FH), and N-GSDMD from each group. **(B)** The release of IL-1 $\beta$ , IL-18, and TNF- $\alpha$  in the supernatant was detected by ELISA. **(C)** The level of LDH release in the supernatant. **(D)** The ASC speck-like protein was detected by immunofluorescence. Scale bars, 5  $\mu$ m. **(E)** Representative images of APC-Annexin-V and PE-PI double staining were used to assess programmed cell death measured by flow cytometry. **(F)** The cells were dual-stained with FLICA and PI and photographed with a fluorescence microscope. The Hoechst 33,342 was used to stain nuclei (Blue). Scale bar, 20  $\mu$ m. The NLRP3-KO mice and WT mice were subjected to CLP or sham surgery. Moreover, some WT mice were randomized and treated intraperitoneally with DNase 1 before CLP surgery (n = 6). **(G and I)** The relative levels of NLRP3, caspase-1, caspase-1 p20, GSDMD, and N-GSDMD relative to the control GAPDH expression in the different groups of the lung tissues were measured by Western blot. **(H and K)** Representative NLRP3 immunohistochemical staining images in lung tissues are shown. Scale bar, 50  $\mu$ m and 100  $\mu$ m. The level of NLRP3 was quantified by AOD using Image-Pro Plus 6.0 software. **(J)** Pathological injuries in the lungs tissues from different groups are shown by H&E staining. Scale bar, 50  $\mu$ m and 100  $\mu$ m. For all experiments, data are presented as the mean  $\pm$  SD, one-way ANOVA was used for statistical analysis, \*P < 0.05, \*\*P < 0.01. **Abbreviation:** ns, not significant (p > 0.05).



( $p < 0.01$ ) (Figure 3C). However, blocking NLRP3 with MCC950 significantly downregulated LDH release and the level of pyroptosis-associated proteins ( $p < 0.01$ ) (Figure 3A–C). These results indicated that NETs-induced AM pyroptosis was dependent on NLRP3 activation. As reported previously, GSDMD can indirectly enhance NLRP3 inflammasome activation,<sup>38</sup> and the GSDMD inhibitor disulfiram (DSF) could remarkably inactivate the NLRP3 inflammasome complex assembly and LDH release (Figure 3A–C). ASC speck formation plays a central role in pyroptosis.<sup>39</sup> ASC speck-like proteins were observed in the LPS + NETs group but were absent after treatment with MCC950 or DSF (Figure 3D). Flow cytometry assays showed that the cell death rate was highest in the LPS + NETs group ( $p < 0.01$ ) (Figure 3E). Furthermore, double-staining for PI + active caspase-1 was used to identify pyroptosis. The results were consistent with the above conclusion (Figure 3F). To further verify whether NETs mediate NLRP3 inflammasome activation and pyroptosis in vivo, intraperitoneal injection of DNase I was used to restrain NETs formation. As expected, haematoxylin and eosin (H&E) staining showed that DNase I administration significantly mitigated the lung histopathologic changes in septic mice (Figure 1D). Furthermore, the protein expression levels of NLRP3, caspase-1 p20, and N-GSDMD in lung tissues were significantly decreased ( $p < 0.01$ ) (Figure 3G). Moreover, IHC analysis further provided evidence that DNase I treatment decreased the expression of NLRP3 in lung tissues of septic mice ( $p < 0.01$ ) (Figure 3H). Collectively, disruption of NETs alters the course of septic lung injury progression. Notably, the levels of NLRP3, caspase-1 p20, and N-GSDMD determined by Western blot analysis were higher in the CLP group than in the sham group ( $p < 0.01$ ) (Figure 3G and I). However, compared to the gene knockout control group, the CLP-treated NLRP3-knockout group showed almost undetectable levels of NLRP3 (Figure 3I); this expression was also significantly decreased in the CLP-treated GSDMD-knockout group (Figure S1A). Notably, the expression of N-GSDMD and Caspase-1 p20 was remarkably suppressed in the CLP-treated NLRP3 and GSDMD knockout groups ( $p < 0.01$ ) (Figure 3I, S1A). Moreover, H&E staining suggested that lung injury was not readily induced after CLP in NLRP3- or GSDMD-knockout mice compared to knockout control mice (Figure 3J, S1B). Similarly, IHC assays showed strong expression of NLRP3 in the CLP groups, while NLRP3 was almost absent in the CLP-treated NLRP3-knockout group and significantly decreased in the CLP-treated GSDMD-knockout groups (Figure 3K, S1C). In summary, the above results demonstrate that NETs induce AM pyroptosis by activating the NLRP3 inflammasome, downregulating NETs or targeting components of the NLRP3 inflammasome to effectively attenuate sepsis-induced lung injury.

## NETs Trigger NLRP3 Deubiquitination to Induce NLRP3 Activation

To detect NLRP3 deubiquitination, confocal microscopy was used to detect the fluorescence intensity in NR8383 cells. The results suggested that the fluorescent signal for the NLRP3 protein in the LPS + NETs group was noticeably enhanced, accompanied by a reduction in the fluorescent signal for ubiquitin; this pattern was distinct from those in the other groups (Figure 4A). Immunoprecipitation assays further showed that the polyubiquitination of NLRP3 was significantly inhibited in the LPS + NETs group (Figure 4B). G5, an inhibitor of deubiquitinating enzymes,<sup>35</sup> restored the ubiquitination level of NLRP3 and inhibited the formation of the NLRP3-ASC complex induced by LPS in combination with NETs (Figure 4A–C). Then, we investigated whether NETs can affect NLRP3 deubiquitination to stimulate the activation of the NLRP3 inflammasome and downstream pyroptosis pathways. LPS-primed NR8383 cells were exposed to NETs for up to 12 h, and G5 or phosphate-buffered saline (PBS) was added 15 min prior to NETs addition. The expression of pyroptosis-associated proteins, such as NLRP3, Caspase-1 p20, and N-GSDMD, was markedly decreased in the LPS + NETs + G5 group compared to the inhibitor control group ( $p < 0.01–0.05$ ) (Figure 4D). G5 significantly depressed the levels of IL-1 $\beta$ , IL-18, and LDH release ( $p < 0.01$ ) in the supernatant but not that of TNF- $\alpha$  ( $p > 0.05$ ) (Figure 4E and F). Moreover, G5 administration trivially formed ASC foci, as detected by confocal microscopy (Figure 4G). Similarly, cell death rates (Figure 4H) and the number of pyroptotic AM (Figure 4I) were remarkably decreased in the LPS + NETs + G5 groups, as assessed by a microscopy assay and flow cytometry assay, respectively. Overall, the above results indicate that NLRP3 deubiquitination plays a vital role in NETs-induced NLRP3 inflammasome activation and AM pyroptosis.

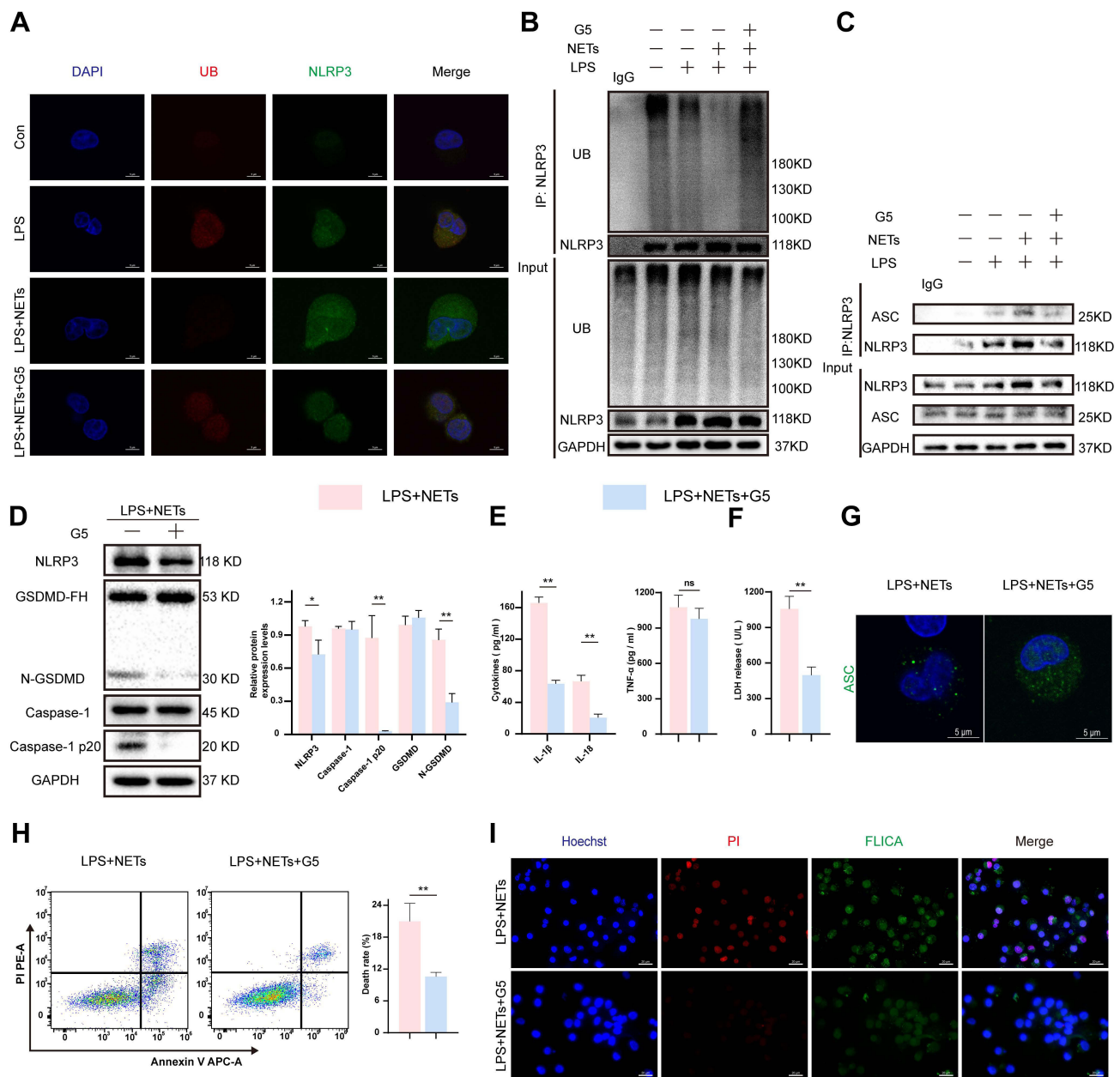


**Figure 4** NETs trigger the deubiquitination of NLRP3 to activate NLRP3. LPS-primed NR8383 cells were treated with NETs for 12 h. G5 (1 μM) was added 15 min prior to NETs. **(A)** Confocal microscopy was used to analyze NLRP3 and ubiquitin fluorescence signals from four groups. ubiquitin (red), NLRP3 (green). Scale bar, 5 μm. **(B)** Western blot analysis of NLRP3 ubiquitination in cell lysates immunoprecipitated with anti-NLRP3 beads, rabbit IgG was regarded as control. **(C)** The level of NLRP3 and ASC protein detected by immunoblot analysis in cell lysates immunoprecipitated with anti-NLRP3 antibody, rabbit IgG as control. **(D)** Western blot showing the levels of pyroptosis associated proteins in whole-cell lysates. **(E and F)** The IL-1β, IL-18, TNF-α, and LDH release in the supernatant. **(G)** Immunofluorescence staining showed the ASC foci formation. Scale bar, 5 μm. **(H)** Cell death rate was assessed by flow cytometry. **(I)** Representative immunofluorescence images of pyroptotic AM from indicated groups. Scale bar, 50 μm. For all experiments, data are presented as the mean ± SD, unpaired Student's t-test was used for statistical analysis, \*P < 0.05, \*\*P < 0.01. **Abbreviation:** ns, not significant (p > 0.05).

## NETs Promote NLRP3 Deubiquitination by Triggering ROS Accumulation

ROS are indispensable in the activation of NLRP3 inflammasome in response to various stimuli.<sup>23</sup> To validate the level of ROS bursts in the cytoplasm in each group, flow cytometry was performed and revealed that the proportion of DCFH-DA-positive cells in the LPS + NETs group reached up to 80% and that the positive rate decreased significantly when the NETs were degraded (p < 0.01) (Figure 5A and B). A similar conclusion was reached with the immunofluorescence assay (Figure 5C). Accordingly, NETs were concluded to significantly upregulate ROS production in NR8383 cells.

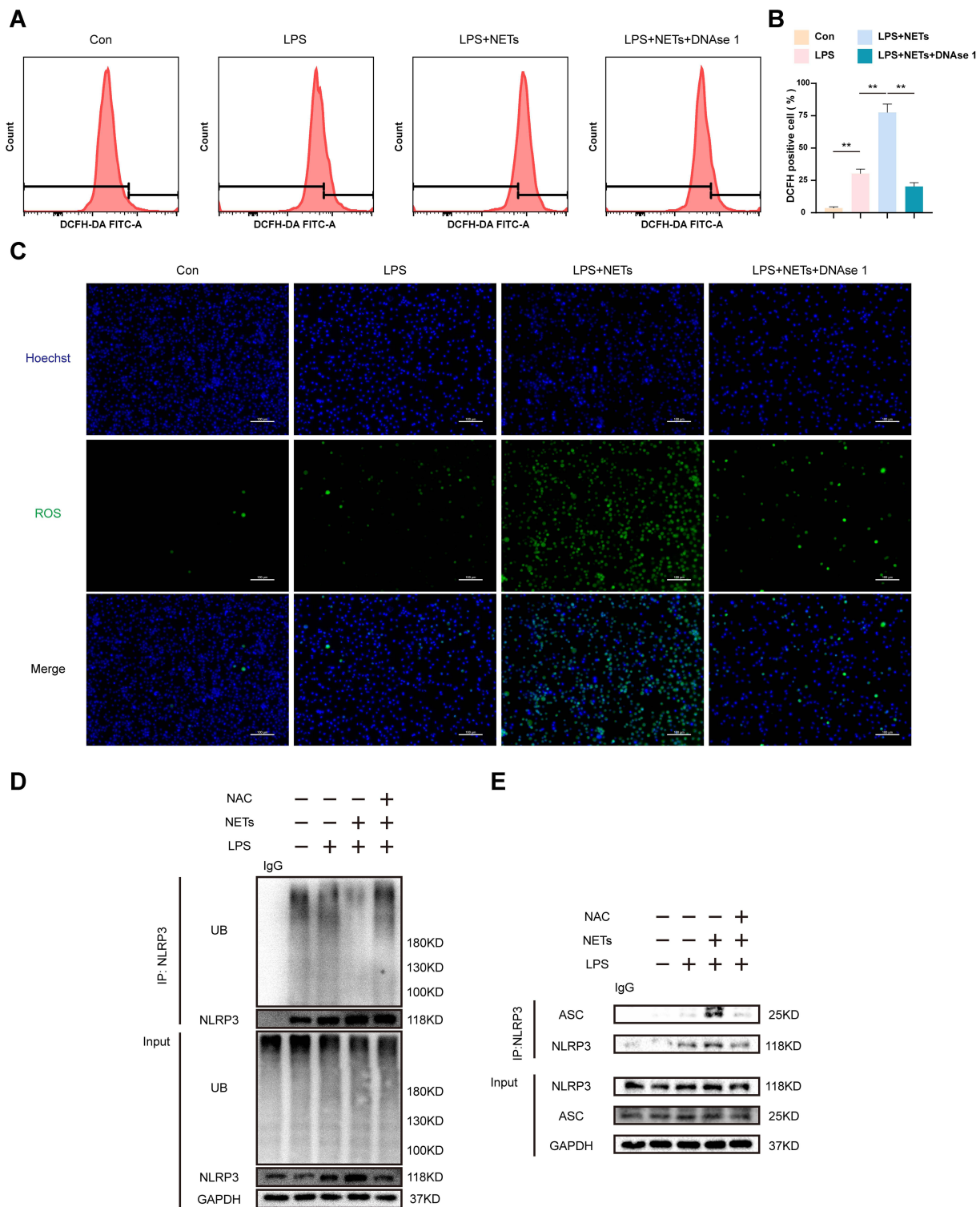


**Figure 5** NETs regulate NLRP3 inflammation activation via mediating ROS generation. LPS-primed NR8383 cells were stimulated with NETs in the presence or absence of DNase 1. **(A)** Flow cytometry showing representative histograms of ROS production labelled by DCFH-DA fluorescence in each group. **(B)** Quantitative analysis of DCFH DA-positive cell ratio. **(C)** ROS production (green) was evaluated with immunofluorescent staining. The nuclei were counterstained with Hoechst 33,342 (Blue). Scale bar, 100  $\mu$ m. LPS-primed NR8383 cells were treated with NAC (10 mM) for 1 h, followed by NETs up to 12 h. **(D)** Cell extracts collected from each group were subjected to immunoprecipitation assays with anti-NLRP3 beads, followed by immunoblotting with an anti-ubiquitin antibody, rabbit IgG was regarded as control. **(E)** Immunoblot analysis of NLRP3 and ASC protein in cell lysates immunoprecipitated with anti-NLRP3 antibody, rabbit IgG was regarded as control. For all experiments, data are presented as the mean  $\pm$  SD, one-way ANOVA was used for statistical analysis, \*\*P < 0.01.

**Abbreviation:** ns, not significant ( $p > 0.05$ ).

Subsequently, we utilized N-acetylcysteine (NAC), a scavenger of ROS, to explore the effect of ROS on the ubiquitination of NLRP3. We found that NAC markedly increased the binding of NLRP3 to ubiquitin molecules, inhibiting NLRP3 deubiquitination induced by LPS + NETs, as measured by coimmunoprecipitation and immunoblot assays (Figure 5D). Furthermore, the formation of the NLRP3-ASC complex was significantly reduced in the LPS+NETs+NAC group (Figure 5E). In brief, these findings indicate that NETs can mediate NLRP3 deubiquitination activation in AM by increasing ROS production.

## NAC Can Inhibit AM Pyroptosis and Ameliorate Lung Injury

Subsequently, we examined whether NAC limits AM pyroptosis *in vitro*. Immunoblot assays revealed that the expression levels of NLRP3, caspase-1 p20, and N-GSDMD were notably decreased in the LPS + NETs + NAC group ( $p < 0.01$ – $0.05$ ) (Figure 6A). Moreover, as detected by ELISA, NAC administration immensely suppressed the release of IL-1 $\beta$ , IL-18, and LDH ( $p < 0.01$ ) (Figure 6B and C) into the supernatant. In contrast, there was no apparent difference in the TNF- $\alpha$  level ( $p > 0.05$ ) (Figure 6B). Furthermore, treatment with NAC eliminated ASC speck formation detected by confocal microscopy (Figure 6D). Likewise, compared to the effect of an inhibitor control, the protective effect of NAC resulted in a significant decline in the proportion of AM undergoing programmed cell death (Figure 6E) or pyroptosis (Figure 6F). Then, we investigated the anti-inflammatory effect of NAC in sepsis-induced lung injury via intraperitoneal injection of NAC prior to CLP modelling. We found that NAC administration significantly mitigated lung injury in septic mice (Figure 6G and I). Moreover, the protein expression levels of NLRP3, caspase-1 p20, and N-GSDMD measured by immunoblot assays and IHC staining were notably decreased in CLP mice pretreated with NAC ( $p < 0.01$ ) (Figure 6H, J and K). In short, the generation of intracellular ROS is a critical cause of NETs-induced AM pyroptosis and lung injury.

## Discussion

Sepsis is a common indirect factor for the progression of lung injury.<sup>40</sup> The interaction between neutrophils undergoing NETosis and macrophages plays a central role in ALI,<sup>41,42</sup> but the exact mechanisms remain poorly understood. Our study confirmed that activated neutrophils released NETs as a medium of communication between immune cells to induce AM pyroptosis and generate inflammatory cytokines to worsen sepsis-induced lung injury. Briefly, NETs increased the burst of ROS in AM. Then, the flood of ROS participated in the assembly of NLRP3 inflammasomes by regulating NLRP3 deubiquitination activation, leading to caspase-1 activation and AM pyroptosis to facilitate the release of bulk IL-1 $\beta$  and IL-18, thereby exacerbating lung injury progression (Figure 7). Moreover, DNase 1, a common inhibitor of NETs, prevented NETs-induced AM pyroptosis and reduced lung inflammation in CLP mice.

Emerging evidence has revealed that NETs are produced systemic inflammatory diseases. For example, NETs stimulate lung epithelial cells to release inflammatory factors, further enhancing the recruitment of immune cells and the production of NETs at inflammatory sites.<sup>43</sup> Additionally, NETs induce a macrophage phenotype transition to trigger scar tissue formation post epidural fibrosis and aggravate ARDS.<sup>41,44</sup> In our study, we found a large amount of NETs production and IL-1 $\beta$  secretion in the lung tissue of septic mice. However, these events were markedly inhibited in septic mice pre-treated with DNase 1. Additionally, the infiltration of neutrophils and macrophages was increased in the lung tissue of septic mice, and these cells were adjacent in space, which provides for the possibility of mutual interaction between NETs and macrophages. In addition, NETs were induced and isolated to validate their proinflammatory effects *in vitro*. We observed that the secretion of IL-1 $\beta$  and IL-18 was considerably increased in AM stimulated with LPS plus NETs but significantly diminished when NETs were digested. These results indicate that NETs could stimulate an inflammatory response in AM.

Macrophage pyroptosis has an essential role in septic lung injury, while the caspase-1 inhibitor Ac-YVAD-CMK inhibits pyroptosis to alleviate LPS-induced ALI in mice.<sup>45</sup> We observed that NETs upregulated the expression of pyroptosis-related proteins *in vivo* and *in vitro*. Moreover, co-stimulation with NETs and LPS induced ASC speck formation in AM, facilitating caspase-1 activity and ultimately leading to a marked elevation in the number of pyroptotic cells. In addition, disruption of NETs or NLRP3 inflammasome-related proteins could effectively impede AM pyroptosis and alleviate lung injury. These results jointly indicate that NETs are effective activators of the NLRP3 inflammasome complex. Notably, lung damage was remarkably alleviated in DNase 1-treated septic mice. First, the local high-



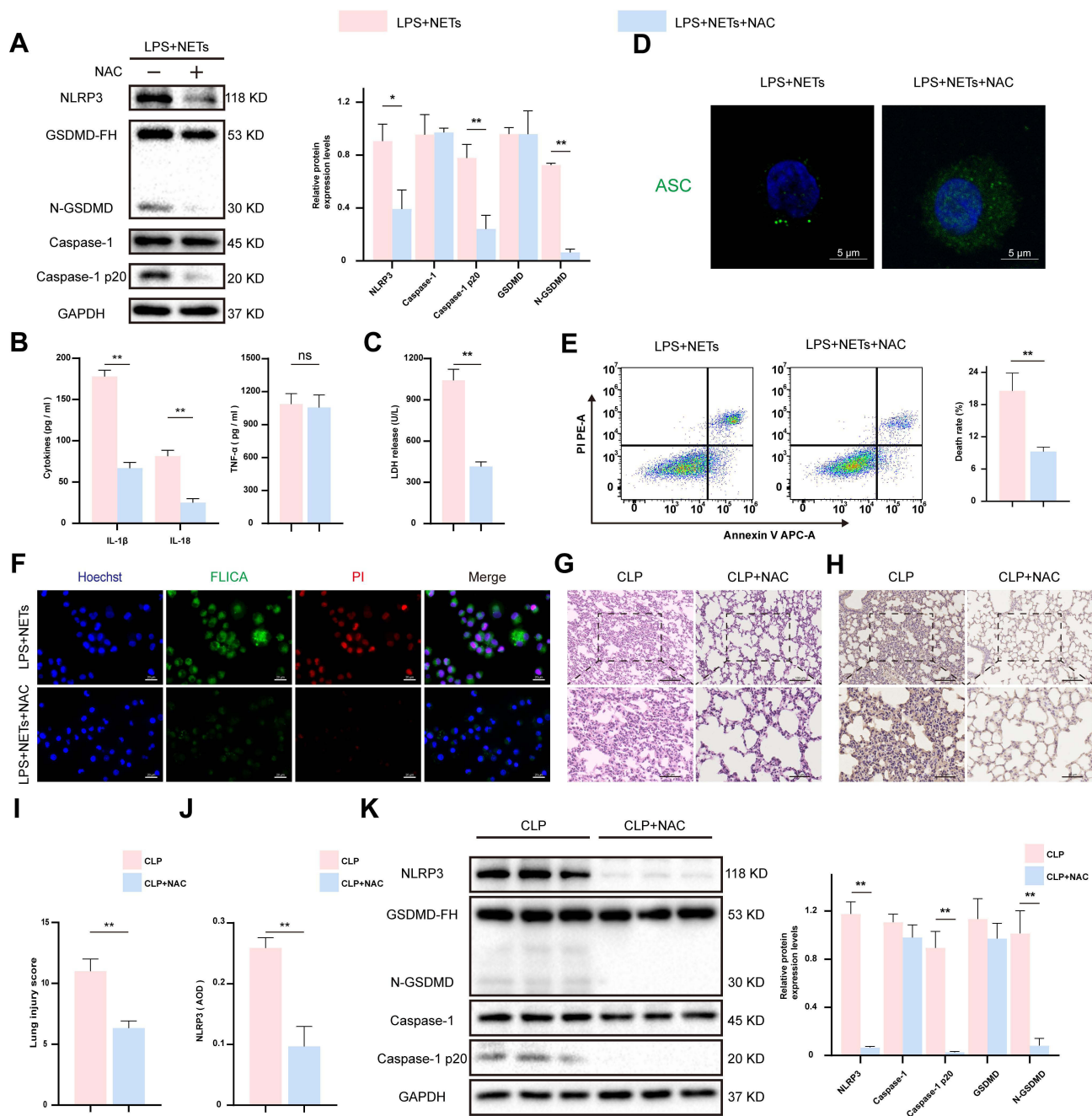


**Figure 6** The ROS scavenger NAC suppressed AM pyroptosis and ameliorated lung inflammation. LPS-primed NR8383 cells were treated with NAC for 1 h, followed by NETs for up to 12 h. **(A)** Western blot showing the levels of pyroptosis associated proteins in cell lysates. **(B and C)** The IL-1 $\beta$ , IL-18, TNF- $\alpha$ , and LDH release in the supernatant. **(D)** ASC speck formation was observed with immunofluorescence staining. Scale bar, 5  $\mu$ m. **(E)** The frequency of programmed cell death was assessed by flow cytometry assay. **(F)** Immunofluorescence staining showed pyroptotic AM from the indicated groups. Scale bar, 20  $\mu$ m. Intraperitoneal injection of NAC at 1 h prior to the CLP model was established (n = 6). **(G and I)** H&E staining showed pathological lung tissue injuries from each group. Scale bar, 50  $\mu$ m and 100 $\mu$ m. **(H and J)** Immunohistochemistry assay for the expression of NLRP3 in lung tissues. Protein was quantified by AOD using Image-Pro Plus 6.0 software. Scale bar, 50  $\mu$ m and 100 $\mu$ m. **(K)** The expression of pyroptosis-associated proteins was detected by Western blotting assay in lung tissues of mice. For all experiments, data are presented as the mean  $\pm$  SD, unpaired Student's t-test was used for statistical analysis, \*P < 0.05, \*\*P < 0.01.

**Abbreviation:** ns, not significant (p > 0.05).

concentration protein network surrounded by chromatin fibres was destroyed by DNase 1. Second, the integrity of NETs was lost, which prevented macrophage engulfment of NETs and subsequent pyroptosis pathway activation.

The activation of NLRP3 inflammasomes in macrophages is a two-step process. The mRNA levels of IL-1 $\beta$  and NLRP3 are upregulated under stimulation by priming signals, which provides a “material base” for downstream molecular events.



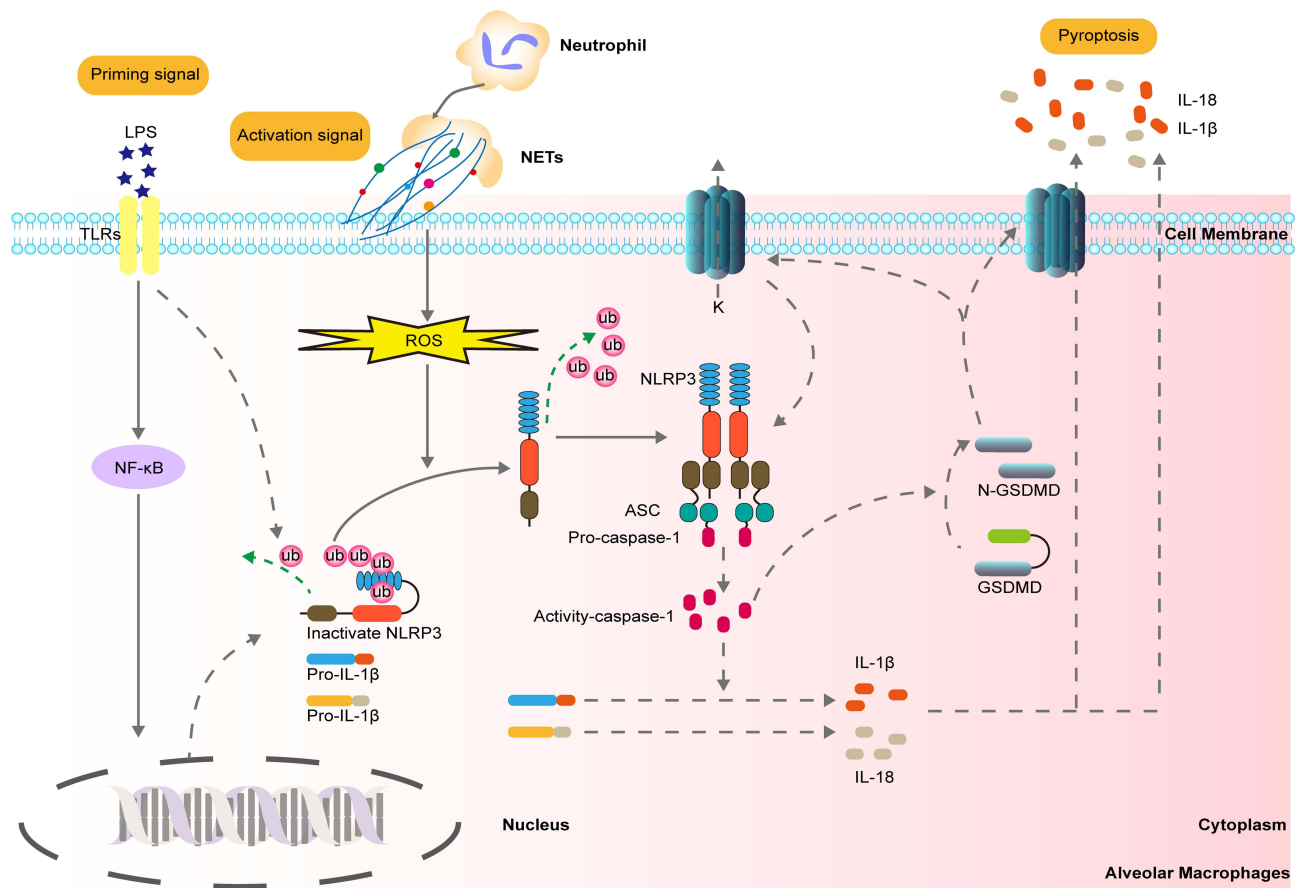


**Figure 7** Schematic diagram of the signaling pathway in which NLRP3 inflammasome activation and AM pyroptosis regulated by NETs. Activating the NLRP3 inflammasome in macrophages requires dual-signal stimulation. In addition to upregulating NLRP3 and IL-1 $\beta$  at the transcriptional level, LPS can also cause partial ubiquitin chain shedding from the NLRP3 protein. Meanwhile, activated neutrophils release NETs as the second signal of alveolar macrophage activation, which stimulates ROS production in macrophages, causing the conformational change of NLRP3 protein and the removal of polyubiquitin chains, thereby leading to NLRP3 inflammasome assembly, caspase-1 activation, AM pyroptosis and a large number of inflammatory factors release.

Subsequently, the activation signal causes the intracellular assembly and activation of the NLRP3 inflammasome to promote mature IL-1 $\beta$  release.<sup>46</sup> Studies have reported that both the priming and activation signals promote NLRP3 inflammasome assembly by regulating NLRP3 deubiquitination.<sup>28</sup> The function of the NLRP3 inflammasome is significantly inhibited by promoting NLRP3 ubiquitination.<sup>31,47</sup> Likewise, deubiquitination of NLRP3 can be inhibited by celastrol to reduce caspase-1 activity and the secretion of IL-1 $\beta$ , which is beneficial for alleviating the liver injury induced by LPS/*Propionibacterium acnes*.<sup>48</sup> These studies have highlighted that deubiquitination events are critical in the activation of the NLRP3 inflammasome. Then, we demonstrated that NETs activated the pyroptosis pathway, which is related to the deubiquitination of NLRP3, in AM. NETs disturb the interaction between ubiquitin molecules and NLRP3 to facilitate the deubiquitination of NLRP3. Moreover, the deubiquitinase inhibitor G5 can restore the binding between NLRP3 and ubiquitin. Notably, multiple experimental results showed that G5 reduced the expression levels of NETs-induced pyroptosis-related indicators and the number of pyroptotic AM. Therefore, NETs induce NLRP3 inflammasome activation by affecting NLRP3 deubiquitination to mediate AM pyroptosis and further promote the inflammatory response in septic mice.

Our study further clarified the potential mechanism and the effect of NETs on NLRP3 deubiquitination. We observed that NETs significantly promoted ROS generation in AM but were substantially reduced with DNase 1 treatment. Consistent with our experimental results, ROS are an essential intermediate in the activation of the NLRP3 inflammasome through multiple signalling pathways.<sup>49</sup> However, targeted ROS production can inhibit NLRP3-mediated colitis-related cancers.<sup>31</sup> Moreover, through coimmunoprecipitation studies evaluating AM stimulated by LPS plus NETs, we found that the binding of ubiquitin molecules to NLRP3 was deficient and that NLRP3 ubiquitination was significantly restored with a ROS scavenger. NAC suppressed the formation of the NLRP3 inflammatory complex, hindered the activation of downstream functional proteins,

and further inhibited IL-1 $\beta$  maturation and AM pyroptosis. Accordingly, we speculated that targeting ROS generation and NLRP3 deubiquitination activation may be a novel strategy for inhibiting NETs-induced macrophage pyroptosis and treating sepsis-induced lung injury. For the first time, we studied the stimulatory effect of NETs on NLRP3 inflammasome activation at the post-translational modification level and clarified the critical role of NLRP3 deubiquitination reliant upon ROS regulation in AM pyroptosis and septic lung injury.

## Conclusion

In conclusion, we found that NETs induced NLRP3 deubiquitination to promote the assembly and activation of the NLRP3 inflammasome, depending mainly on the generation of ROS caused by multiple intracellular cascade effects, which in turn promoted AM pyroptosis and released a large number of inflammatory factors, potentially leading to the progression of septic lung injury. Our research identifies a novel mechanism by which NETs function in AM pyroptosis and provides an effective therapeutic strategy to treat septic lung injury.

## Funding

This work was supported by the National Natural Science Foundation of China (82160363 and 81871548).

## Disclosure

The authors declare that they have no competing interests.

## References

1. Singer M, Deutschman CS, Seymour CW, et al. The third international consensus definitions for sepsis and septic shock (sepsis-3). *JAMA*. 2016;315(8):801–810. doi:10.1001/jama.2016.0287
2. Sevransky JE, Levy MM, Marini JJ. Mechanical ventilation in sepsis-induced acute lung injury/acute respiratory distress syndrome: an evidence-based review. *Crit Care Med*. 2004;32(11 Suppl):S548–553. doi:10.1097/01.CCM.0000145947.19077.25
3. Sadowitz B, Roy S, Gatto LA, Habashi N, Nieman G. Lung injury induced by sepsis: lessons learned from large animal models and future directions for treatment. *Expert Rev Anti Infect Ther*. 2011;9(12):1169–1178. doi:10.1586/eri.11.141
4. Mikkelsen ME, Shah CV, Meyer NJ, et al. The epidemiology of acute respiratory distress syndrome in patients presenting to the emergency department with severe sepsis. *Shock*. 2013;40(5):375–381. doi:10.1097/SHK.0b013e3182a64682
5. Park I, Kim M, Choe K, et al. Neutrophils disturb pulmonary microcirculation in sepsis-induced acute lung injury. *Eur Respir J*. 2019;53(3):1800786. doi:10.1183/13993003.00786-2018
6. Brinkmann V, Reichard U, Goosmann C, et al. Neutrophil extracellular traps kill bacteria. *Science*. 2004;303(5663):1532–1535. doi:10.1126/science.1092385
7. Papayannopoulos V. Neutrophil extracellular traps in immunity and disease. *Nat Rev Immunol*. 2018;18(2):134–147. doi:10.1038/nri.2017.105
8. Fuchs TA, Abed U, Goosmann C, et al. Novel cell death program leads to neutrophil extracellular traps. *J Cell Biol*. 2007;176(2):231–241. doi:10.1083/jcb.200606027
9. Liu S, Su X, Pan P, et al. Neutrophil extracellular traps are indirectly triggered by lipopolysaccharide and contribute to acute lung injury. *Sci Rep*. 2016;6(1):37252. doi:10.1038/srep37252
10. Zha C, Meng X, Li L, et al. Neutrophil extracellular traps mediate the crosstalk between glioma progression and the tumor microenvironment via the HMGB1/RAGE/IL-8 axis. *Cancer Biol Med*. 2020;17(1):154–168. doi:10.20892/j.issn.2095-3941.2019.0353
11. Josefs T, Barrett TJ, Brown EJ, et al. Neutrophil extracellular traps promote macrophage inflammation and impair atherosclerosis resolution in diabetic mice. *JCI Insight*. 2020;5(7):e134796. doi:10.1172/jci.insight.134796
12. Liu D, Yang P, Gao M, et al. NLRP3 activation induced by neutrophil extracellular traps sustains inflammatory response in the diabetic wound. *Clin Sci*. 2019;133(4):565–582. doi:10.1042/CS20180600
13. Kahlenberg JM, Carmona-Rivera C, Smith CK, Kaplan MJ. Neutrophil extracellular trap-associated protein activation of the NLRP3 inflammasome is enhanced in lupus macrophages. *J Immunol*. 2013;190(3):1217–1226. doi:10.4049/jimmunol.1202388
14. Deng Q, Pan B, Alam HB, et al. Citrullinated histone H3 as a therapeutic target for endotoxemic shock in mice. *Front Immunol*. 2019;10(2020):2957. doi:10.3389/fimmu.2019.02957
15. Lefrancais E, Mallavia B, Zhuo H, Calfee CS, Looney MR. Maladaptive role of neutrophil extracellular traps in pathogen-induced lung injury. *JCI Insight*. 2018;3(3):e98178. doi:10.1172/jci.insight.98178
16. Yipp BG, Petri B, Salina D, et al. Infection-induced NETosis is a dynamic process involving neutrophil multitasking in vivo. *Nat Med*. 2012;18(9):1386–1393. doi:10.1038/nm.2847
17. Vande Walle L, Lamkanfi M. Pyroptosis. *Curr Biol*. 2016;26(13):R568–R572. doi:10.1016/j.cub.2016.02.019
18. He WT, Wan H, Hu L, et al. Gasdermin D is an executor of pyroptosis and required for interleukin-1 $\beta$  secretion. *Cell Res*. 2015;25(12):1285–1298. doi:10.1038/cr.2015.139
19. Man SM, Karki R, Kanneganti TD. Molecular mechanisms and functions of pyroptosis, inflammatory caspases and inflammasomes in infectious diseases. *Immunol Rev*. 2017;277(1):61–75. doi:10.1111/imr.12534
20. Howrylak JA, Nakahira K. Inflammasomes: key mediators of lung immunity. *Annu Rev Physiol*. 2017;79(1):471–494. doi:10.1146/annurev-physiol-021115-105229

21. Luo D, Dai W, Feng X, et al. Suppression of lncRNA NLRP3 inhibits NLRP3-triggered inflammatory responses in early acute lung injury. *Cell Death Dis.* 2021;12(10):898. doi:10.1038/s41419-021-04180-y
22. Wang L, Lei W, Zhang S, Yao L. MCC950, a NLRP3 inhibitor, ameliorates lipopolysaccharide-induced lung inflammation in mice. *Bioorg Med Chem.* 2021;30(8):115954. doi:10.1016/j.bmc.2020.115954
23. Tschopp J, Schroder K. NLRP3 inflammasome activation: the convergence of multiple signalling pathways on ROS production? *Nat Rev Immunol.* 2010;10(3):210–215. doi:10.1038/nri2725
24. Hu Q, Shi H, Zeng T, et al. Increased neutrophil extracellular traps activate NLRP3 and inflammatory macrophages in adult-onset Still's disease. *Arthritis Res Ther.* 2019;21(1):9. doi:10.1186/s13075-018-1800-z
25. Bednash JS, Mallampalli RK. Regulation of inflammasomes by ubiquitination. *Cell Mol Immunol.* 2016;13(6):722–728. doi:10.1038/cmi.2016.15
26. Lopez-Castejon G, Luheshi NM, Compan V, et al. Deubiquitinases regulate the activity of caspase-1 and interleukin-1beta secretion via assembly of the inflammasome. *J Biol Chem.* 2013;288(4):2721–2733. doi:10.1074/jbc.M112.422238
27. Ren G, Zhang X, Xiao Y, et al. ABRO1 promotes NLRP3 inflammasome activation through regulation of NLRP3 deubiquitination. *EMBO J.* 2019;38(6):e100376. doi:10.15252/embj.2018100376
28. Juliana C, Fernandes-Alnemri T, Kang S, et al. Non-transcriptional priming and deubiquitination regulate NLRP3 inflammasome activation. *J Biol Chem.* 2012;287(43):36617–36622. doi:10.1074/jbc.M112.407130
29. Abais JM, Xia M, Zhang Y, Boini KM, Li PL. Redox regulation of NLRP3 inflammasomes: ROS as trigger or effector? *Antioxid Redox Signal.* 2015;22(13):1111–1129. doi:10.1089/ars.2014.5994
30. Xia X, Shi Q, Song X, et al. Tetrachlorobenzoquinone stimulates NLRP3 inflammasome-mediated post-translational activation and secretion of IL-1beta in the HUVEC endothelial cell line. *Chem Res Toxicol.* 2016;29(3):421–429. doi:10.1021/acs.chemrestox.6b00021
31. Dai G, Jiang Z, Sun B, et al. Caffeic acid phenethyl ester prevents colitis-associated cancer by inhibiting NLRP3 inflammasome. *Front Oncol.* 2020;10(2020):721. doi:10.3389/fonc.2020.00721
32. Xu J, Jiang Y, Wang J, et al. Macrophage endocytosis of high-mobility group box 1 triggers pyroptosis. *Cell Death Differ.* 2014;21(8):1229–1239. doi:10.1038/cdd.2014.40
33. Toscano MG, Ganea D, Gamero AM Cecal ligation puncture procedure. *J Vis Exp.* 2011;7(51):2860. doi:10.3791/2860
34. Najmeh S, Cools-Lartigue J, Giannias B, Spicer J, Ferri LE. Simplified human neutrophil extracellular traps (NETs) isolation and handling. *J Vis Exp.* 2015;16(98):52687. doi:10.3791/52687
35. Py BF, Kim MS, Vakifahmetoglu-Norberg H, Yuan J. Deubiquitination of NLRP3 by BRCC3 critically regulates inflammasome activity. *Mol Cell.* 2013;49(2):331–338. doi:10.1016/j.molcel.2012.11.009
36. Jin Y, Wu W, Zhang W, et al. Involvement of EGF receptor signaling and NLRP12 inflammasome in fine particulate matter-induced lung inflammation in mice. *Environ Toxicol.* 2017;32(4):1121–1134. doi:10.1002/tox.22308
37. Chi K, Geng X, Liu C, et al. LncRNA-HOTAIR promotes endothelial cell pyroptosis by regulating the miR-22/NLRP3 axis in hyperuricaemia. *J Cell Mol Med.* 2021;25(17):8504–8521. doi:10.1111/jcmm.16812
38. Deng W, Yang Z, Yue H, et al. Disulfiram suppresses NLRP3 inflammasome activation to treat peritoneal and gouty inflammation. *Free Radic Biol Med.* 2020;152(2020):8–17. doi:10.1016/j.freeradbiomed.2020.03.007
39. Stehlik C, Lee SH, Dorfleutner A, et al. Apoptosis-associated speck-like protein containing a caspase recruitment domain is a regulator of procaspase-1 activation. *J Immunol.* 2003;171(11):6154–6163. doi:10.4049/jimmunol.171.11.6154
40. Monahan LJ. Acute respiratory distress syndrome. *Curr Probl Pediatr Adolesc Health Care.* 2013;43(10):278–284. doi:10.1016/j.cppeds.2013.10.004
41. Song C, Li H, Li Y, et al. NETs promote ALI/ARDS inflammation by regulating alveolar macrophage polarization. *Exp Cell Res.* 2019;382(2):111486. doi:10.1016/j.yexcr.2019.06.031
42. Chen X, Li Y, Qin L, He R, Hu C. Neutrophil extracellular trapping network promotes the pathogenesis of neutrophil-associated asthma through macrophages. *Immunol Invest.* 2021;50(5):544–561. doi:10.1080/08820139.2020.1778720
43. Wan R, Jiang J, Hu C, et al. Neutrophil extracellular traps amplify neutrophil recruitment and inflammation in neutrophilic asthma by stimulating the airway epithelial cells to activate the TLR4/NF-κB pathway and secrete chemokines. *Aging.* 2020;12(17):16820–16836. doi:10.18632/aging.103479
44. Jin Z, Sun J, Song Z, et al. Neutrophil extracellular traps promote scar formation in post-epidural fibrosis. *NPJ Regen Med.* 2020;5(1):19. doi:10.1038/s41536-020-00103-1
45. Wu D, Pan P, Liu B, et al. Inhibition of alveolar macrophage pyroptosis reduces lipopolysaccharide-induced acute lung injury in mice. *Chin Med J.* 2015;128(19):2638–2645. doi:10.4103/0366-6999.166039
46. Man SM, Kanneganti TD. Regulation of inflammasome activation. *Immunol Rev.* 2015;265(1):6–21. doi:10.1111/imr.12296
47. Guo C, Xie S, Chi Z, et al. Bile acids control inflammation and metabolic disorder through inhibition of NLRP3 inflammasome. *Immunity.* 2016;45(4):802–816. doi:10.1016/j.immuni.2016.09.008
48. Yan CY, Ouyang SH, Wang X, et al. Celastrol ameliorates Propionibacterium acnes/LPS-induced liver damage and MSU-induced gouty arthritis via inhibiting K63 deubiquitination of NLRP3. *Phytomedicine.* 2021;80(2021):153398. doi:10.1016/j.phymed.2020.153398
49. Dostert C, Pétrilli V, Van Bruggen R, et al. Innate immune activation through nalp3 inflammasome sensing of asbestos and silica. *Science.* 2008;320(5876):674–677. doi:10.1126/science.1156995